REAL-TIME EXTRACTION OF HYDRODYNAMIC FLOW CHARACTERISTICS USING SURFACE SIGNATURES

Siva M. Mangalam
Tao Systems (www.taosystem.com)
Williamsburg, VA 23185
(757) 220-5040, siva@taosystem.com

Abstract

Biological creatures like birds and fish appear to use surface (skin) sensors and integrated actuators for efficient propulsion and maneuvers. They seem to be well equipped to effectively extract energy from the non-stationary surrounding medium. Advanced design of biorobotic underwater autonomous vehicles will require instantaneous sensing of hydrodynamic forces in response to biomimetic actuators.

The present paper describes recent advances in measurement techniques that can be used to sense surface signatures for real-time extraction of important hydrodynamic flow phenomena such as boundary-layer transition from laminar-to-turbulent flow, flow-separation, and vortex dynamics. These surface signatures can be calibrated to obtain skin friction drag and unsteady hydrodynamic forces generated by lifting bodies. The same system can also used to determine speed and flow angularity of the body in motion relative to the surrounding medium. These advances provide unprecedented opportunities for the development of adaptively controlled biorobotic systems with high performance and safety features. The paper presents a few selected examples from recent wind tunnel, and flight experiments that were conducted by Tao Systems to validate the innovative approach.

Introduction

Viscous effects and unsteady hydrodynamics play a dominant role in the performance, safety, and control of underwater autonomous vehicles (UAV). Real-time sensing and extraction of hydrodynamic flow characteristics are important for the design and performance of underwater autonomous and biorobotic vehicles with efficient bio-propulsion and adaptive maneuver control capabilities.

The fundamental mathematical equations for hydrodynamics were developed by late nineteenth century and completed by the first decade of the 20th century. It is about a hundred years since the introduction of Prandtl's boundary layer theory [1]. Enormous progress has been made during this period. Nevertheless, we still do not have reliable and universally acceptable methods to predict and control many of the most critical flow phenomena such as boundary-layer transition, flow separation, cavitation, and turbulence. The problem becomes even more pronounced in three-dimensional and unsteady flows.

Critical Hydrodynamic Flow Phenomena that affect vehicle performance are

(a) Speed
(b) Attitude (flow angularity)
(c) Laminar-to-Turbulent Transition
(d) Turbulence
(e) Flow Separation with or without Reattachment
(f) Cavitation
(g) Vortex dynamics
(h) Unsteady Interactions between the Structure (Vehicle) and Flow Oscillations

Conventional approaches to obtain these hydrodynamic phenomena are generally complex, expensive, and intrusive even for simple steady flow conditions. They also often require off-surface measurements to characterize the flow-field for comparison with computational codes, which are primarily based on Navier-Stokes (N-S) equations. The dependent variables in N-S equations are the three components of velocity, pressure, temperature, viscosity, and thermal conductivity. Historically, experimental techniques have been geared towards the extraction of these variables through point measurements. For efficient operation, and closed-loop active control of biorobotic autonomous underwater vehicles (AUV) will require all these measurements *simultaneously and in real time* around complex bodies in unsteady flows. Conventional measurement approach is clearly unwieldy for such applications.

In a number of projects supported by NASA and DOD SBIR/STTR Programs spanning over nearly a decade, Tao Systems has introduced innovative techniques to simultaneously identify and monitor characteristic surface signatures associated with important flow phenomena in real time. Tao Systems has developed a simple and more robust engineering approach to identify flow phenomena from surface signatures and relate them to vehicle performance characteristics. These innovations are described in the following sections with representative examples from experiments.

Measurement Approach

It is well known that viscous effects cause momentum transfer through hydrodynamic phenomena like boundary-layer transition, turbulence, separation, and skin friction. These viscous effects are most dominant at the fluid-structure interface, i.e. at the vehicle skin. Viscous effects and pressure gradients directly impact the state of the boundary layer (laminar, transitional, or turbulent) and its ability to stay attached to the surface. The vehicle propulsion system has to overcome these effects for effective and safe maneuvers. The vehicle performance and safety depend largely upon how these hydrodynamic phenomena are sensed and controlled.

Critical hydrodynamic flow features (CHyFF) manifest themselves in two important ways (the important hydrodynamic phenomenon of cavitation is not considered in this paper):

(a) Boundary-layer transition from laminar to turbulent flow and
(b) Flow bifurcation: leading-edge stagnation point (LESP), flow separation and reattachment, vortex formation and shedding.

These phenomena have a direct impact on hydrodynamic drag and lift. The skin-friction drag is directly dependent on boundary-layer transition and turbulence. Bifurcation regions have dramatic effect on both lift and pressure drag of AUV's.

Our measurement approach has been to extract surface signatures that characterize these important hydrodynamic phenomena resulting from the fluid-structure interactions. The fluid imparts momentum to the surface (and vice versa) in fundamentally three mutually perpendicular directions. They manifest themselves as pressure in a direction normal to the surface and as shear stress (skin friction) in a direction tangential to the surface. There are well-established methods to make normal pressure measurements. Here we shall focus on relative shear stress measurements and describe how such measurements can be related to hydrodynamic flow phenomena and to the forces and moments generated by the vehicle.

The measurement system consists of an array (or matrix) of waterproofed hot-film sensors embedded on flexible substrates that could be glued on to the vehicle surface to form its outer skin. A bank of automated high-sensitivity, large bandwidth constant voltage anemometers to operate surface hot-film sensors, and signal processing software / hardware to extract critical hydrodynamic flow features.

Sensors

A typical sensor array consists of a number of 0.25 micron-thin nickel-sensor elements and 2-microns-thick copper leads (Fig. 1.) vacuum deposited on a flexible, insulated substrate. These sensors are arranged as per user requirement. For example, the sensor shown in Fig. 1 is made up of a matrix of 8 x 8 sensor elements. Such a configuration is useful for measuring surface signatures on a three-dimensional body with flow changes occurring in both the streamwise and crossflow directions. A simpler array with sensor elements arranged only in the streamwise direction is generally used for 2-dimensional flows.

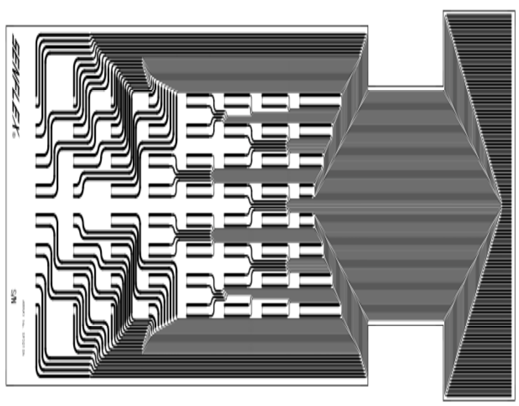

Figure 1. **8 x 8 Hot-Film Sensor Matrix.**

The resistance of the hot-film sensor is a function of the geometry of the element and the operating temperature. In hot-film anemometry, the sensor is initially heated to a value sufficiently above the ambient flow. This temperature gradient allows heat to be transferred to the flow by convection and to the substrate (and the test article) through conduction. The heat lost to the flow through convective heat transfer is a measure of the surface flow conditions. Thermal anemometry deals with the operation of such sensors and interpretation of signals obtained as a result of heat transfer.

Constant Voltage Anemometer (CVA)

Until 1990, two types of anemometers were in widespread use in fluid dynamic measurements: constant current anemometer (CCA) and constant temperature anemometer (CTA). The former maintained the sensor at a prescribed constant current (by suitably changing the voltage across it to account for the change in resistance (temperature) due to heat transfer). The CTA maintains the sensor at a constant resistance (temperature). These two types of anemometers were extensively used in fluid mechanics research for over seven decades. These anemometers require fine-tuning to deal with changes in ambient conditions. They are also susceptible to the adverse impact of EMI and EFI. These and other shortcomings (e.g., cable capacitance effects) restricted their use primarily to research under controlled laboratory conditions.

The introduction of constant voltage anemometer (CVA) in early 90's changed the scenario [2, 3]. The basic circuit diagram for CVA is shown in figure 2.

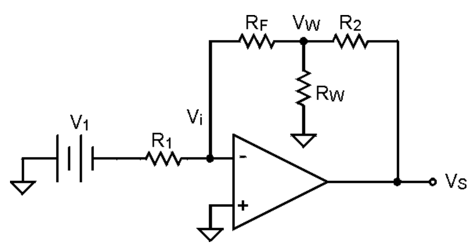

Figure 2. **Basic Circuit for Constant Voltage Anemometer (CVA)**

The voltage V_w across a hot-film sensor with initial resistance (R_w) is maintained constant. The changes in sensor temperature due to changes in flow conditions at the sensor location results in changes in its resistance and a corresponding change in the current through the sensor. This change in current is dropped across a large resistor R_2 to produce a large output voltage. Thus the circuit produces a large front-end sensitivity. The bandwidth of the system is large because it depends primarily on the open-loop gain of the op-Amp.

The CVA design has been successfully used in a number of wind tunnel, water tunnel, ocean, and flight tests covering the entire speed range from low subsonic to hypersonic speeds [4-10]. CVA does not require critical adjustments to account for changes in flow conditions, provides a flat, customer-specified bandwidth, has high signal-to-noise ratio, is practically immune to EMI, RFI, and cable-capacitance effects. It lends itself to complete hands-off automation and miniaturization (Fig. 3).

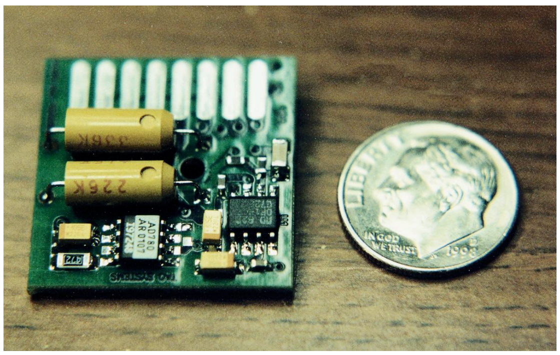

Figure 3. Miniaturized CVA

Unlike CTA and CCA, which are primarily laboratory tools, **CVA can be used as a high-quality laboratory instrument and also for routine engineering applications.**

Surface Signatures of Critical Hydrodynamic Flow Features (CHyFF)

Critical hydrodynamic flow features (CHyFF) manifest themselves essentially in two ways. (a) Boundary-Layer Transition and (b) Flow Bifurcation (flow separation and reattachment, vortex formation and shedding)

Boundary-layer transition (**BLT**) (Fig. 4) from laminar to turbulent flow is determined using one or all the various well-established techniques based on peak RMS signal, intermittency factor, skewness, and spectral density. It is well known that signals from the laminar region have very low disturbance (RMS) levels. Also, the mean wall shear stress (skin friction) in a laminar region is much lower than the wall shear stress in the transitional and turbulent regions. This situation translates to lower mean (DC) output voltage levels in the laminar region compared to transitional and turbulent regions. Intermittency level is a normalized expression of relative turbulence levels. It is computed as a ratio of the time duration when the flow is turbulent to the total sample time. According to this criterion, the laminar flow will exhibit nearly zero intermittence whereas a turbulent flow will have an intermittence of nearly one.

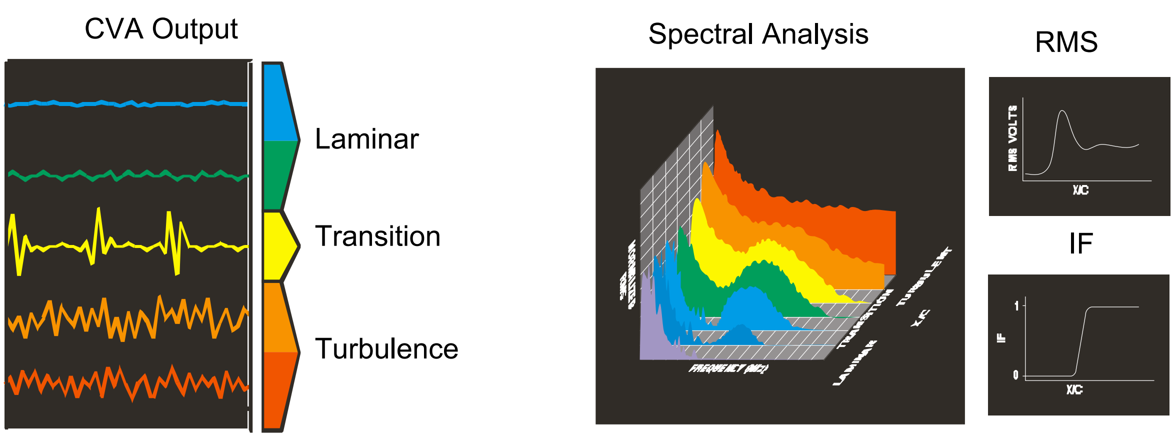

Figure 4. Surface Signatures of Boundary Layer Transition

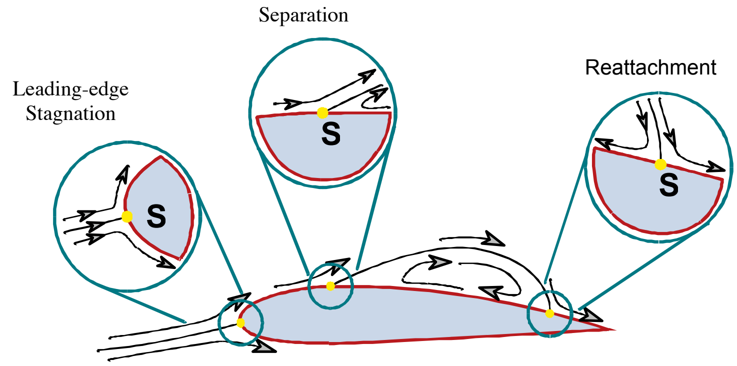

Figure 5. Flow Bifurcation Points

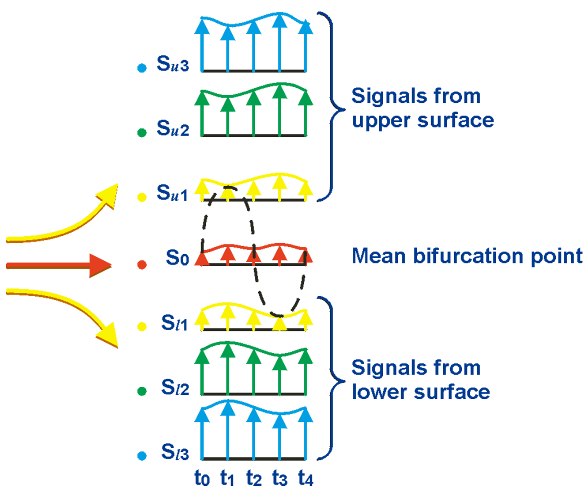

Figure 6. Surface Signatures Near A Bifurcation Point

Flow Bifurcation Points (**FBP**) occur when the flow attaches to or separates from the body. Flow separation and vortex shedding occur primarily due to the inability of the flow to negotiate large pressure gradient. Under certain conditions, the separated vortex flow could also reattach itself to the body. Figure 5 shows an idealized picture of flow features at bifurcation region (S). It is seen that the leading-edge stagnation point (LESP), flow separation, and flow reattachment points all share a common feature: the local streamlines bifurcate in opposite directions resulting in a local minimum in shear stress (and convective heat transfer).

When a hot-film is located at such a point (S), the convective heat transfer from it is a minimum whereas sensors located away from such points experience increased shear stress and heat transfer.

In real flows, FBP moves back and forth due to flow unsteadiness with corresponding changes in sensor outputs. CVA output signals from hot-film sensors located in the neighborhood of FBP exhibit certain telltale characteristics as shown in Fig. 6. Here, for clarity, the sensors are shown spread out, with the sensor s_0 located at the mean FBP. At time t_0, when the instantaneous bifurcation streamline is at s_0, the CVA output from this sensor will have a minimum voltage because there is little heat convection. The other sensors will get relatively more cooled because of greater convective heat transfer to the flow. Hence, as the flow accelerates from FBP the output voltages from sensors will increase with distance from the FBP. At time t_1, if we assume that the instantaneous FBP has moved to the sensor location s_1, we should expect the minimum voltage signal to occur at this sensor location. Similar changes take place as the instantaneous FBP moves back and forth, as shown by the dashed line.

The locus of arrowheads at each sensor location represents CVA output signal (time series) at each spatial location. We can observe the following features:

(a) The CVA output signal from sensor located at the mean FBP exhibits the lowest mean output voltage compared to sensors on either side of it.
(b) Signals from sensors located on one side of the bifurcation point are in phase.
(c) Signals from sensors located across FBP exhibit a phase-reversal signature.
(d) The sensor located at the mean FBP exhibits a double frequency for every cycle.

A similar picture is obtained in the presence of streamwise or crossflow vortices, which introduce alternate regions of high and low shear stresses. As in the case of FBP's described above, these vortices also tend to be unsteady and leave a similar pattern of signals in a direction normal to the direction of the vortices.

These features were verified in a number of experiments conducted in wind tunnel, water tunnel, in flight, and on ocean-going vessels. In a flight test conducted by NASA Dryden Flight Research Center [7], hot-film sensors were installed on a transonic airfoil mounted on F-15B flight test fixture (see photos shown below).

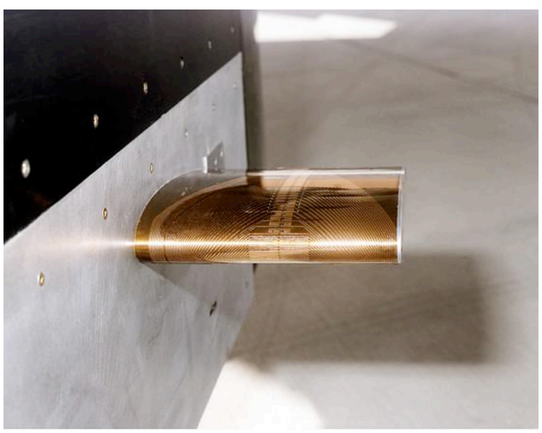

The sensor layout is shown in Fig. 7a. The model shown in Fig. 7b was instrumented with 60 hot-film sensors and pressure sensors. For clarity, Figure 7c shows raw signals only from hot-film sensors 21, 22, and 23. These signals correspond to the presence of shock-induced separation at transonic speeds. It is clear that the signals from sensors 21 and 23 are out of phase while the signal from the sensor 22 (shown in

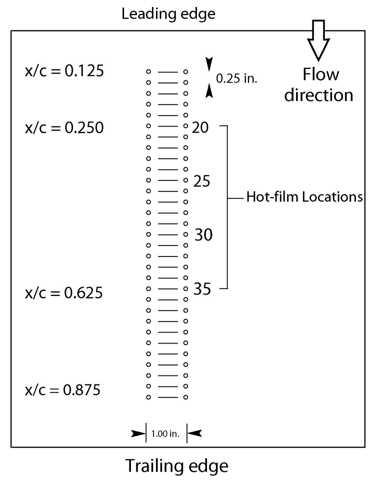

Figure 7a. Flight-tests on F-15B: Sensor Layout

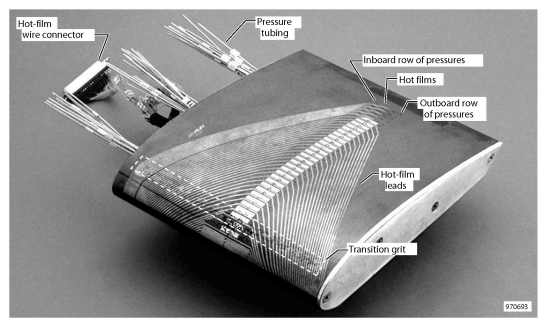

Figure 7b. Instrumented Airfoil Model

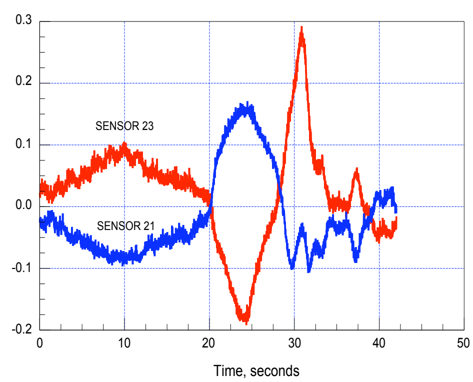

Figure 7c. CVA Output Voltages from Sensors #21 and #23

Fig. 7d), exhibits the double frequency. These signals correspond to one cycle of alpha maneuver.

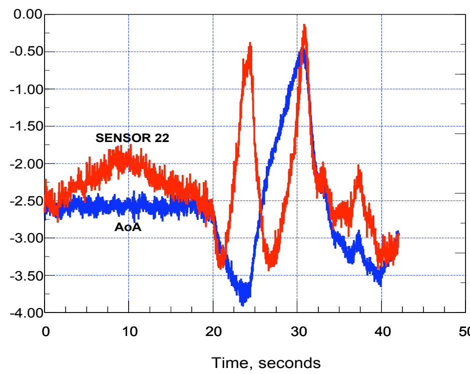

Figure 7d. CVA Output Voltages from Sensor #22 (blue line indicates changes in aircraft angle of attack).

Thus, we conclude that mean FBP was located at the sensor 22 during the maneuver. This conclusion was independently verified by simultaneous pressure measurements [7]. It should be noted that the output signal from a sensor decreases as FBP approaches it and the output increases when the FBP moves away from it. Thus, while the shock-induced separation is initially located between sensors 21 and 23, it first moves towards sensor 21 till t ~ 10 seconds (indicated by decreasing voltage) and then moves away (indicated by increasing voltage) from it and towards the sensor 23. The shock-induced separation reaches the sensor 23 at t ~25 seconds (minimum voltage) and then moves away from it and back towards sensor 21 after t = 25 seconds.

These flight-test results clearly validated our physical modeling of surface signatures caused by FBP.

Experiments on Oscillating Airfoil Models: Tao Systems has developed on-line measurement capability to simultaneously obtain all unsteady viscous phenomena on a dynamically pitching airfoil model. Successful tests were conducted on NACA 0012 model at IIT (Chicago) and USAFA (Colorado Springs) and on an Eppler-387 model under simulated Martian environment in NASA Langley's supersonic tunnel.

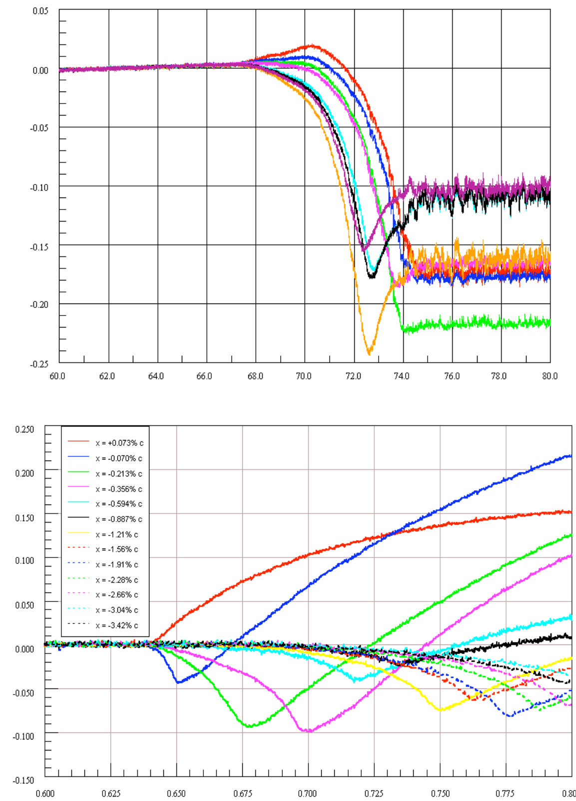

Figure 8. CVA Signals from Sensors on a Dynamically Pitching Airfoil.
(a) Composite plot (top) and
(b) Instantaneous Location & Movement of Bifurcation Points (bottom).

A typical composite plot and some details from such experiments are shown in the following figures (Fig. 8a and b). The output voltage levels are initially auto-zeroed in order to provide a level starting condition for all sensor outputs. The instantaneous location (indicated by voltage minimum for each sensor and phase reversal between neighboring sensors) and systematic movement of the bifurcation point followed by transition to turbulence are clearly seen (Fig. 8a and b). All the relevant surface flow features such as the LESP, separation and reattachment points, and boundary-layer transition location on the airfoil were thus available at each instant of time.

Instantaneous angle-of-attack and side slip angle: The location of the LESP corresponds to the instantaneous angle-of-attack (AOA) of the wing section. When the airfoil model is in the vertical plane (as in the case of an aircraft fin), its LESP will correspond to sideslip angle (SSA). These concepts were used to develop electronic angle of attack and sideslip angle devices [6, 8]. The new LESP-based AOA device is different from conventional pressure-based or mechanical (vanes) AOA systems in a number of respects:

(a) The conventional AOA device gives global AOA with respect to the aircraft longitudinal axis whereas the LESP-based device can provide both global and local (at a given wing/tail section) AOA/SSA.
(b) The LESP-based device with practically instantaneous response is particularly effective in the presence of unsteady maneuvers, buffet, flutter, and flow disturbances. Conventional devices suffer from large time lags.
(c) The LESP-based AOA also can be used as a stall-warning device.
(d) The LESP-based device can provide high resolution compared to conventional AOA devices.
(e) The LESP-based device is non-intrusive, compact, and has no moving parts.

Thus, the unique approach briefly described above makes it possible to identify the instantaneous location as well as the direction of motion of complex viscous phenomena without a priori sensor calibration. The location and direction of motion of FBP's (LESP, flow separation, etc.) can be used as control inputs for actuators in an active feedback control system.

Unsteady Aerodynamic Forces from Surface Signatures

Under a NASADFRC SBIR Phase II program [4], wind tunnel experiments were conducted at the US Air Force Academy (USAFA) test facility under a Cooperative Research & Development Agreement (CRDA) between USAFA and Tao Systems. A picture of the 6"-chord, 18"-span NACA 0015 airfoil model wind-tunnel model instrumented with pressure and hot-film sensors is shown in Fig. 9.

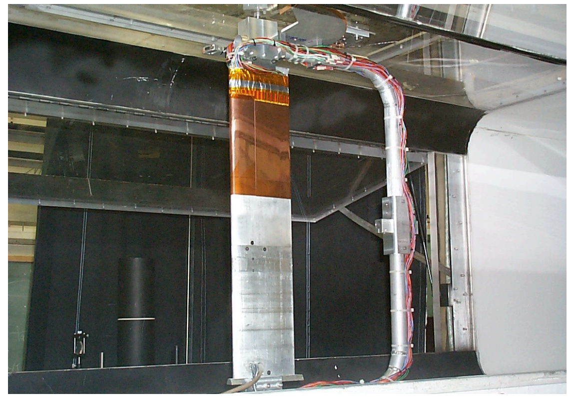

Figure 9. Instrumented Airfoil Model with Oscillation Test Rig Mounted in the USAFA Wind-Tunnel Test Section.

Since the airfoil was symmetrical, the model was instrumented on one surface only with 14 pressure orifices to obtain lift. The airfoil model was also instrumented with 104 hot-film sensors. A special rig was designed to oscillate the airfoil model at different frequencies. The amplitude and frequency of oscillations was computer controlled. The airfoil model and the oscillation rig, including the software for computer-controlled operation were designed at USAFA.

Test Conditions: Wind tunnel tests were conducted at three different speeds (50 fps, 75 fps, and 100 fps) and at various angles of attack from –40 to +40 degrees. Initially tests were conducted at steady-state conditions. These tests were used to obtain steady-state lift coefficient as a function of angle-of-attack using surface pressure distribution. These were followed by tests in which the airfoil was oscillated at different amplitudes and frequencies.

Test Results: The lift generated by the airfoil at each angle was determined from the surface pressure distribution. Hot-film surface signatures were used to determine LESP, transition, flow separation points at each angle-of-attack. As expected, we found that, the changes in the LESP movement with angle-of-attack strongly correlated with lift coefficient (Fig. 10). The movement of FSP from the trailing edge towards the leading-edge region also correlated well with lift coefficient until just beyond the leading-edge stall (Fig. 11).

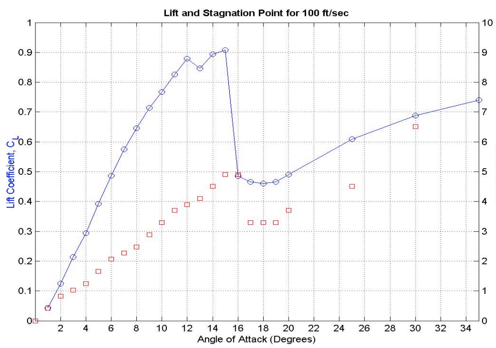

Figure 10. Movement of LESP with Angle-of-attack and Lift Coefficient.

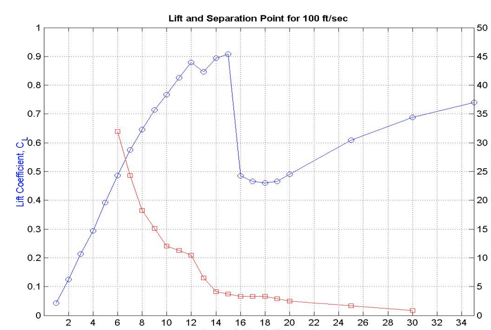

Figure 11. Flow Separation Point Movement with Angle-of-attack and Lift Coefficient

We used these data to fit a polynomial function for lift coefficient in terms of the LESP and flow separation locations. The coefficients of the polynomial were obtained from test data at different angles of attack and free stream velocities. The next question was whether the same polynomial expression can be used to obtain unsteady lift by inserting the instantaneous locations of LESP and flow separation points. Tests were then conducted by oscillating the airfoil at different frequencies. The instantaneous CAFFI locations were obtained using Tao Systems' proprietary hardware and software. Lift coefficients at various test conditions were independently determined from surface pressure distribution.

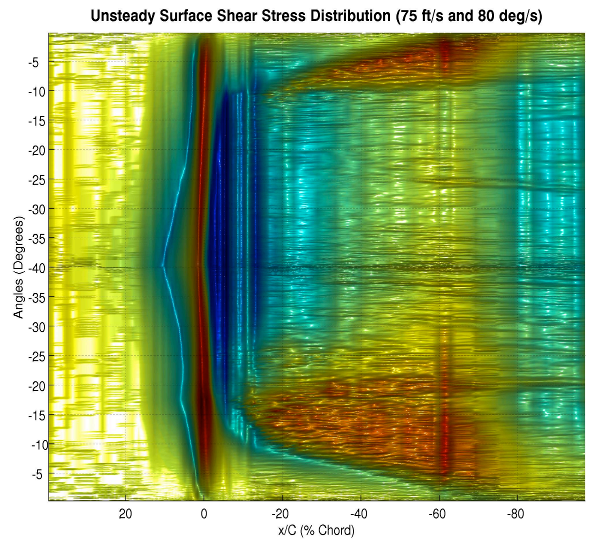

Figure 12. Surface Shear Stress Signatures on the Pitching Airfoil Model

Figure 12 is a graphic illustration of surface signatures as the airfoil completes one cycle of pitching oscillation at 80 degrees per second and a free stream velocity of 75 fps. Since the test model was mounted vertically, the "pitch up" and pitch-down" motions were actually from side to side. However, for convenience we have used conventional terminology to describe the oscillations. The abscissa is chord location of the hot-film sensor and the ordinate is the instantaneous angle-of-attack. Positive and negative chord locations are used to indicate pressure and suction surfaces of the airfoil. The negative sign for the angle of attack indicates that the model was swung to the left from an angle-of-attack of zero degrees to 40 degrees and then back to zero. The color-coding is based on the CVA output voltage, which is a function of surface shear stress. The blue color indicates low shear stress (low convective heat transfer from the hot-films to the surrounding medium of air and red indicates relatively larger surface shear stress region.

Figure 12 shows that the LESP is initially located near the leading edge (blue line at 0% chord) and then moves along the pressure surface (to the left) up to about 15 degrees, when stall occurs. Up to this point the LESP movement resembles the lift curve with angle of attack. During the same period, the separation point moved from the trailing edge towards the leading edge (the second blue line with a more shallow slope). The separation point reaches the leading edge at about 18 degrees when the airfoil is stalled. The separation stays near the leading edge all the way to 40 degrees while the LESP moves further back after remaining practically stationary for a short duration.

The movement of LESP and flow separation points follow a similar trend during the return stroke (pitch down) but compared to the pitch up motion, their actual locations along the airfoil chord are quite different. The airfoil stalls at a much lower angle of attack, closer to 10 degrees when the flow separation occurs at the leading edge of the airfoil. It is also possible to observe high shear regions (indicated by red). If needed, these regions can be further analyzed to locate boundary-layer transition to turbulence. Thus, we were able to capture, in real time, all CAFFI characteristics from surface signatures.

Variation in lift coefficient during pitch up and pitch down motion of airfoil based on pressure distribution are shown in Fig. 13. Figure 14 shows the variation in instantaneous LESP during the same test conditions. Clearly, the trends are similar both during pitch up and pitch down motions. As expected, the lift coefficient shows increased lift during pitch up (blue line) and a marked decrease during the pitch down (red line) motion. The figure 13 also exhibits almost identical trends (the blue symbols indicate LESP locations during pitch up motion and the red symbols represent LESP during pitch down motion).

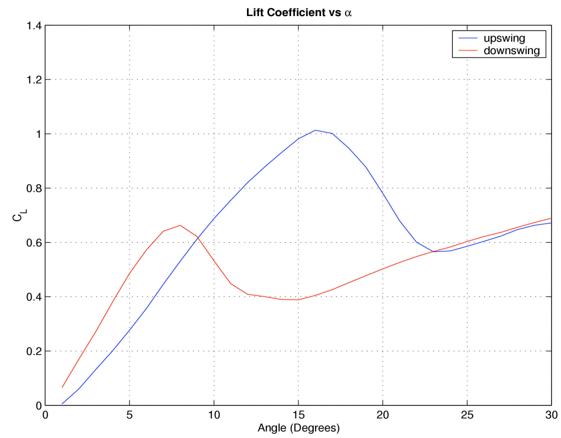

Figure 13. Variation in Lift Coefficient with Angle-of-attack during Pitch-up (red line) and Pitch-down Motions

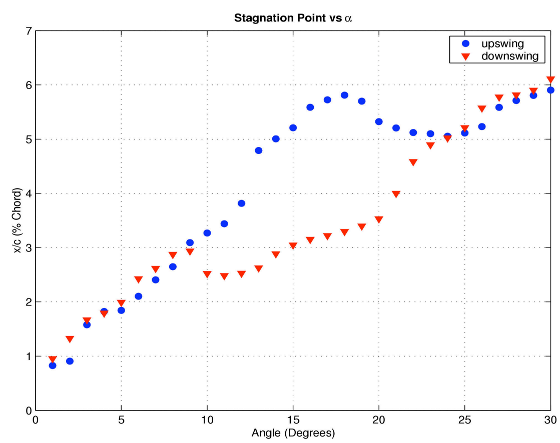

Figure 14. Movement of LESP with Angle-of-attack at the Same Test Conditions as in Fig. 13.

We then used the polynomial expressions from steady-state conditions and inserted these instantaneous values of LESP and flow separation points to determine instantaneous lift coefficient based on surface signatures (Fig. 15). The polynomial expression is given at the top left hand corner. The expression at the bottom of the figure is used for post-stall conditions. It is clear that the LESP and FSP locations are uniquely determined at each flow condition and their locations can be used to obtain the actual lift generated by the lifting body. Similar results were obtained at other pitch rates.

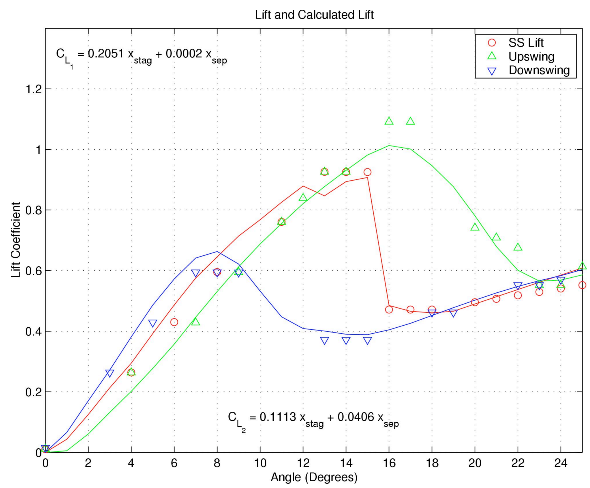

Figure 15. A Comparison of Measured Lift Coefficient with Lift Coefficient Obtained with Surface Signatures of LESP and FSP during Pitch-up ad Pitch-down Oscillations.

Underwater Experiments with Waterproofed Sensors

Tao Systems has developed waterproofed flexible hot-film sensors for underwater applications. Successful experiments were conducted on racing sailboats AmericaOne and Oracle Racing that competed for the America's Cup Challenge. These experiments on the keel and rudder of the sailboats were conducted under practical marine environment off the coasts of California and Auckland, New Zealand. Results from these investigations have not been produced here in view of their proprietary nature.

Tao Systems and Newport News Shipbuilding conducted successful water tunnel tests on a hydrofoil at the Naval Surface Warfare Center (Carderock Division) to demonstrate the capability of obtaining ChyFF from surface signatures using waterproofed hot-film sensors and CVA. Some results from these tests were published in [10].

These successful experiments have shown that it is possible to obtain hydrodynamic flow features from surface hot-film signatures.

Conclusion

Successful wind tunnel, water tunnel, flight-tests, and underwater tests on marine vehicles have shown that CHyFF can be obtained in real time using surface hot-film signatures. Our experiments have shown that a strong correlation exists between real-time CHyFF and unsteady hydrodynamic forces. It is possible to calibrate and sense unsteady hydrodynamic loads merely from surface signatures. In other words, these advances provide opportunities to develop technology to sense like fish and use the sensed quantity as input for control actuators. Such an approach can lead to the development of robust and intelligent biomimetic control systems for biorobotic AUV's.

Acknowledgment

The author gratefully acknowledges active support and encouragement received from Mr. Tim Moes and NASA Dryden Flight Research Center (NAS4-01030) and the support provided by the USAFA under CRDA. The author also thanks his colleagues at Tao Systems for their contributions. Dr. Promode Bandyopadhyay's (ONR) support and encouragement to present this paper at the Biorobotics Workshop is gratefully acknowledged.

References

[1] Schlichting, H. and Gersten, K.: Boundary layer Theory, Springer (2000).

[2] *Flow Rate Measuring Apparatus,(Constant Voltage Anemometer),* US Patent 5074147, Dec. 1991.

[3] *A High Sensitivity, Large Bandwidth Constant Voltage Anemometer,* Final Report, NAS1-20192, NASA LaRC (1996).

[4] *Real time, in-flight determination of unsteady aerodynamic loads and moments*, NASA SBIR Phase II Final Report, NASA DFRC, NAS4-01030 (2003).

[5] Mangalam, S. M., Sarma, G. R., Augustin, M., and Yeary, D.: *Low Speed/Low Cost Airspeed sensor for Helicopters*, 59th American Helicopter Society Forum, Phoenix, AZ, May 2003.

[6] *A Non-intrusive Solid State Angle-of-Attack Instrument,* Final Report, (NAS1-19967, NASA LaRC) (1995)

[7] Moes, T.; Sarma, G. R.; and Mangalam, S. M.: *Flight Demonstration of a Shock Sensor Using Constant Voltage Hot-Film Anemometry*. NASA TM 4806, Aug. 1997.

[8] *Accurate Large Bandwidth Underwater Speed and Flow Angularity Measurement Device,* US Navy SBIR Phase I Final Report, N00024-01-C-4089, NSWC, NAVSEA (2001).

[9] Mangalam, S. M.: *Phenomena-based Real-time Aerodynamic Measurement (PRAM) System for Aircraft Performance, Safety, and Control*, IEE Aerospace Conference, Big Sky, MT, March 2003.

[10] Mangalam, S. M., Sarma, G. R., Pfouts, R. A., Casper, J. H., Wallace, M. A., Moghadam, H. E., snd Nigon, R.: *Detection of Transition and Flow Bifurcation Regions on a Hydrofoil Using Hot-Film Constant Voltage Anemometry,* Proc. Intl. Symposium on Seawater Drag Reduction, Newport, RI, July 1998.